Mechanics & Industry **19**, 312 (2018)

https://doi.org/10.1051/meca/2018001

Mechanics & Industry

Available online at:
www.mechanics-industry.org

Regular Article

Stagnation temperature effect on the supersonic flow around pointed airfoils with application for air

Rahima Takhnouni[1,*], Toufik Zebbiche[2], and Abderrazak Allali[3]

[1] Department of Mechanical Engineering, Faculty of Technology, University of Blida 1, BP 270, Blida 09000 Algeria
[2] Institute of Aeronautics and Space Studies, University of Blida 1, BP 270, Blida 09000 Algeria
[3] Aircraft Laboratory, Institute of Aeronautics and Space Studies, University of Blida 1, BP 270, Blida 09000 Algeria

Received: 3 February 2017 / Accepted: 2 January 2018

Abstract. The aim of this work is to develop a new numerical calculation program to determine the effect of the stagnation temperature on the calculation of the supersonic flow around a pointed airfoils using the equations for oblique shock wave and the Prandtl Meyer expansion, under the model at high temperature, calorically imperfect and thermally perfect gas, lower than the dissociation threshold of the molecules. The specific heat at constant pressure does not remain constant and varies with the temperature. The new model allows making corrections to the perfect gas model designed for low stagnation temperature, low Mach number, low incidence angle and low airfoil thickness. The stagnation temperature is an important parameter in our model. The airfoil should be pointed at the leading edge to allow an attached shock solution to be seen. The airfoil is discretized into several panels on the extrados and the intrados, placed one adjacent to the other. The distribution of the flow on the panel in question gives a compression or an expansion according to the deviation of the flow with respect to the old adjacent panel. The program determines all the aerodynamic characteristics of the flow and in particular the aerodynamic coefficients. The calculation accuracy depends on the number of panels considered on the airfoil. The application is made for high values of stagnation temperature, Mach number and airfoil thickness. A comparison between our high temperature model and the perfect gas model is presented, in order to determine an application limit of the latter. The application is for air.

Keywords: Supersonic flow / pointed airfoil / oblique shock / high temperature / aerodynamic coefficients / Prandtl Meyer function / calorically imperfect gas / thermally perfect gas / specific heat at constant pressure / error of computation

1 Introduction

The aerodynamics study problems on a numerical way is a relatively new research area. Most previous work either theoretical [1–6], or numerical [3,5,7–16] or even experimental in wind tunnel [9] on supersonic flows around airfoils are devoted to rounded airfoils at the leading edge, that is to say a development of a detached shock wave at the leading edge. These studies are generally based on the numerical solution of the Euler equations [1–6] or the equation of potential speed [1,4,5].

The pointed shape of the airfoil at the leading edge gives the possibility of having an attached shock wave, where a numerical technique can be used to evaluate the aerodynamic parameters of the flow. Since the flow is supersonic in the open air, far from the presence of any other obstacle, this technique makes it possible to progressively follow the flow on the airfoil surface as a function of the parameters of the upstream flow.

Given the complexity of the methods used in the supersonic aerodynamics [1–6], and in particular that presented in this study, called a relaxation shock method, the authors use an analytical technique named by thin-airfoil theory [3–6] to evaluate approximately the flow parameters, and in particular the calculation of the aerodynamic coefficients. This method gives acceptable results for very small airfoil thicknesses and upstream Mach number.

The first study on the use of the expansion shock method is presented in reference [17]. This method is used for the calorically and thermally perfect gas. They assume in this case that the specific heat at constant pressure C_P is constant and does not depend on the temperature. This approach gives acceptable results only if the three parameters M_0, T_0 and t/C are very small. It is our opinion that the PG model does not depend on the stagnation temperature T_0.

* e-mail: rahima_takhnouni@yahoo.com

The aim of this work is to develop a new mathematical model and to develop in this context a new numerical calculation program to determine the stagnation temperature effect on the supersonic flow around a pointed airfoil, using the equations of an oblique shock and the Prandtl Meyer expansion in the case at high temperature, calorically imperfect and thermally perfect gas, lower than the dissociation threshold of the molecules, in order to correct the PG model, and to determine the aerodynamic characteristics presented by the lift, drag and pitching moment coefficients as a function of upstream Mach number, incidence angle, airfoil shape and airfoil thickness and especially of the stagnation temperature, when they are high. In this case, the specific heat at constant pressure does not remain constant and varies with the increase in temperature, which will be taken into account in our HT model. The stagnation temperature T_0 is an important parameter in our model, which will demonstrate considerable corrections to the results given by the PG model. The latter gives good results only if the values of M_0, T_0, α, t/C are very small. Then, given the current and future applications in supersonic aerodynamics requiring high values of M_0, T_0 and t/C witch exceeding respectively 2.00, 1000 K and 10.0, and can arrive at 5.00, 3500 K respectively. The PG model falls failing, and the results given by this model becomes very far from the reality, which requires to make corrections to this model, hence the interest of the application of our HT model. We can consider that the HT model becomes a generalization of the PG model. In the other word, the PG model becomes a particular case of our HT model. The PG model falls failing, and the results given by this model becomes very far from the reality, which requires to make corrections to this model, hence the interest of the application of our HT model. We can consider that the HT model becomes a generalization of the PG model, were the application of the HT model is extended to high value of T_0, M_0, α and t/C. The application is for air. In this case and for the C_P function, one finds in references [5,8,9,18,19] a series of a tabulated values for the variation of C_P according to the temperature, between 55 K and 3550 K (limit not to have a dissociation of the molecules). In this temperature margin and according to references [15,16,18,19], only the translational, rotational and chemical vibrational energies are present and are included in the total evaluation of the specific heat $C_P(T)$ of air. Other sources of energy, such as the molecular dissociation energy and the ionization energy of the atoms, are absent since the temperature margin does not exceed 3500 K. A polynomial interpolation is made to these values, after several tests, in order to find an analytic function with the variation of $C_P(T)$ with the temperature. A choice on a 9th degree polynomial is made, giving a maximum error less than 0.01%. More details are found in references [8,9].

2 Mathematical model at high temperature

A flow deviation on the airfoil surface may result in a compression or a Prandtl Meyer expansion. If the compression is produced in the flow, a shock wave develops at the beginning of the deviation of the obstacle as shown in Figure 1. Otherwise, expansion waves develop at the beginning of the deviation as Figure 2 shown it. In both cases, there is a perturbation of the flow which results in a change of all the flow parameters through this deviation. It can be shown that, through the shock, only the total temperature [5,8,9,15,16] is conserved. Then $T_0 = T_{01} = T_{02}$. But the total pressure and density change values. Hence $P_{0_2}/P_{0_1} = \rho_{0_2}/\rho_{0_1} \neq 1.0$.

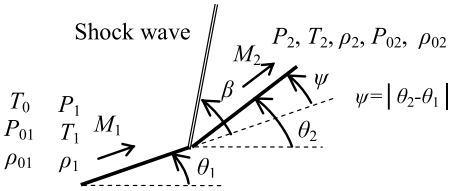

Fig. 1. Compression of an angle ψ.

For the Prandtl Meyer expansion, the temperature and the total pressure will be preserved. We set the conditions at infinity upstream by T_0, ρ_0 and P_0. We assume that the state equation of a perfect gas ($P = \rho RT$) remains valid, with $R = 287.102\,\mathrm{J/(kg\,K)}$. For PG model $\gamma = 1.402$ is taken [8,9,14].

2.1 Oblique shock wave

Figure 1 shows a general diagram of the development of an oblique shock wave at the beginning of the deflection of an obstacle by an angle $\psi = |\theta_2 - \theta_1|$ and the envisaged parameters.

For the determination of the parameters (M_2, β, T_2/T_1, ρ_2/ρ_1, P_2/P_1, P_{0_2}/P_{0_1}, ΔS_{21}) through the oblique shock, the HT model presented in references [10–13] is used *after making a correction to the relation between* β, ψ *and* M_1, since the authors used the equation designed for the PG model to constant C_P [10], given the difficulty of finding an analytic form, which gives results far enough of reality, and that does not meet the need for HT assumptions This equation is the most interesting in the calculation of the shock parameters, since all the other parameters depend on β, ψ and M_1. Then, in the quality of the results, corrections will be found to the results presented in the said references. Another modification made at the $C_P(T)$ level used in these references. It has been observed that $C_P(T)$ used exhibits a slight discontinuity in the passage of $T = 1000$ K with a 27% error between the function used and the tabulated values [18,19].

The relationship can be summarized as follows:

$$\frac{\rho_2}{\rho_1} = \frac{tg(\beta)}{tg(\beta - \psi)}, \tag{1}$$

$$\frac{T_2}{T_1} = \frac{\frac{\rho_2}{\rho_1} - M_1^2 \sin^2(\beta) \times \gamma(T_1) \times \left(1 - \frac{\rho_2}{\rho_1}\right)}{\left(\frac{\rho_2}{\rho_1}\right)^2}, \tag{2}$$

$$\frac{P_2}{P_1} = \left[\frac{T_2}{T_1}\right]\left[\frac{\rho_2}{\rho_1}\right], \tag{3}$$

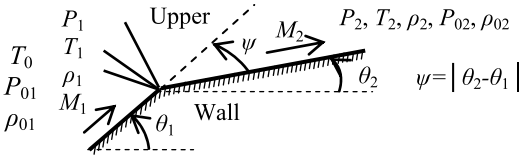

Fig. 2. Expansion of an angle ψ.

$$M_2^2 = \frac{1 - \frac{P_2}{P_1}}{\sin^2(\beta - \psi) \times \gamma(T_2) \times \left[1 - \frac{\rho_2}{\rho_1}\right]\frac{P_2}{P_1}}, \quad (4)$$

$$\frac{\rho_2}{\rho_{0_2}} = \mathrm{Exp}\left(-\int_{T_2}^{T_0} \frac{C_P(T)}{a^2(T)}\, dT\right), \quad (5)$$

$$\frac{P_2}{P_{0_2}} = \left[\frac{T_2}{T_0}\right]\left[\frac{\rho_2}{\rho_{0_2}}\right], \quad (6)$$

$$\frac{P_{0_2}}{P_{0_1}} = \frac{\left[\frac{P_2}{P_1}\right]\left[\frac{P_1}{P_{0_1}}\right]}{\left[\frac{P_2}{P_{0_2}}\right]}, \quad (7)$$

$$\frac{\Delta S_{21}}{R} = -\mathrm{Log}\left(\frac{P_{0_2}}{P_{0_1}}\right), \quad (8)$$

$$\gamma(T) = \frac{C_P(T)}{C_P(T) - R}. \quad (9)$$

Two solutions can be found depending on the value of M_2, implying that all physical parameters will admit two solutions. If $M_2 \geq 1.00$, a weak shock is obtained. If $M_2 < 1.00$, a strong shock is obtained. In general, the weak shock that occurs in nature.

Prior to the determination of the flow parameters by (1–8), we must determine the angle β corresponding to ψ and M_1. Then in this work, we will determine the deviation β with high precision according to the real HT model presented in this work. Since the development of an analytic relation between β, ψ and M_1 is quite complicated, we will use the relations of a normal shock wave to HT model [14].

2.2 Expansion of Prandtl – Meyer

The situation of the presence of a Prandtl Meyer expansion is presented in Figure 2. In this case we will have a deviation of an angle $\psi = |\theta_2 - \theta_1|$. The flow becomes parallel to the wall after the deviation, and the calculation of the parameters after the expansion takes place after the calculation of the new value of the Prandtl Meyer function by the following relation:

$$\nu(T_2) = \nu(T_1) + \psi. \quad (10)$$

The function PM at HT can be calculated by the following equation [20,21]:

$$\nu(T) = \int_T^{T^*} \frac{C_P(T)}{2H(T)} \sqrt{M^2(T) - 1}\, dT, \quad (11)$$

where [8,9]:

$$M(T) = \frac{\sqrt{2H(T)}}{a(T)}, \quad (12)$$

$$a^2(T) = \gamma(T) RT, \quad (13)$$

$$H(T) = \int_T^{T_0} C_P(T)\, dT. \quad (14)$$

First, it is necessary to calculate the critical temperature T^* corresponding to the Mach number $M = 1.00$. This temperature depends only on T_0. It can be determined numerically by solving the nonlinear equation obtained from relation (12) by replacing $M = 1.00$ and $T = T^*$ using the bipartition algorithm [22–24]. We obtain $T^* < T_0$. It is calculated once in the problem.

In equation (10), ψ and T_1 are known. Then $\nu(T_1)$ can be calculated from equation (11) by replacing $T = T_1$. The evaluation of the obtained integral is done by the use of the Simpson quadrature with condensation of the nodes [20] or using the Gauss Legendre quadrature of a function having a weight term to accelerate the numerical process [21]. Let us replace the obtained result in (10) to determine the new value $\nu(T_2)$. Let us replace again this value in (11). In this case we fall into an inverse problem. That is to say, it is necessary to determine the temperature T_2 which gives the integral (11) equal to the value given by (10). To determine T_2 from (11), a combination of the bipartition algorithm with the Gauss Legendre quadrature was used. It should be noted that $T_2 < T^*$. The precision chosen in the calculation is $\varepsilon = 10^{-8}$. In this case, the bipartition algorithm is used 27 times.

Once T_2 is determined, it is possible to obtain the corresponding ratio T_2/T_0 and the Mach number M_2 by relation (12) and ρ_2/ρ_{0_2} and P_2/P_{0_2} respectively by relations (5) and (6). We will have an increase in Mach number, i.e., $M_2 > M_1$. Integration (5) is done by using the Simpson method with nodes condensation [8,9].

3 Numerical procedure

The aim is to determine the aerodynamic characteristics summarized by the variation of M, T/T_0, ρ/ρ_0, P/P_0 along the airfoil surface and consequently the determination of the aerodynamic coefficients C_D, C_L and C_m for different airfoils.

Figures 1 and 2 shows the case of the flow deflection on the extrados. For the intrados, the opposite occurs. To group the problem in a single relation, we used the absolute value for the evaluation of the angle. In the developed program, we first compute the angle $\psi = \theta_2 - \theta_1$. Then, if we are on the extrados, the expansion occurs if $\psi < 0.0$ and the compression occurs if $\psi > 0.0$. The opposite is taken into account on the intrados.

Subdividing the selected airfoil into k nodes on the upper surface and into l nodes in the lower surface as shown in Figure 3. The total number of the nodes on the chosen

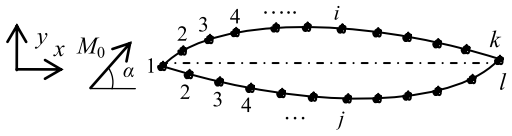

Fig. 3. Airfoil discretization in some panels.

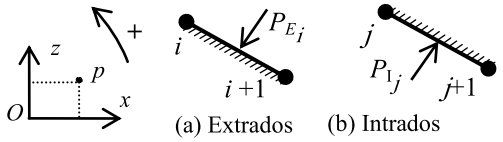

Fig. 4. Presentation of the forces on the segment.

airfoil surface is equal to $n = k + l - 2$. The number of regions on the upper surface is equal to $k-1$ and it is equal to $l-1$ in the lower surface.

A streamline coming from infinity upstream is divided into two parts at the leading edge of the airfoil (point 1). One is through the upper surface and the other through the lower surface, so that the two lines meet again at the trailing edges. We can consider the flow calculation according to the upper part and the lower surface after the other.

Every two juxtaposed panels are connected by a node. At each node, the flow undergoes a deviation by generating either a compression or expansion, or similar continuous across it, Figure 3.

To expansion either on the upper or lower surfaces, it will be an increase in Mach number, that is to say that $M_2 > M_1$. As against a compression will decrease the Mach number $M_2 < M_1$. Since it was considered that the shock is weak (real case).

Note that these parameters are constant along the segment for the shock and expansion. The flow properties in a region on the right are function of the flow parameters in the region of the left. Since these are known. There may be a detached shock if the angle ψ exceed the angle $\psi_{\max}$.

The jump in entropy is zero for an expansion [1–6]. For a compression, the entropy is different to zero. The relation (8) gives the variation of the entropy between the passages from one adjacent segment to another. To determine the total flow leap around the airfoil, all the local entropy leaps must be summed.

We may encounter a cases where the flow on the upper and lower surfaces has no deviation, i.e., $\psi = (\theta_2 - \theta_1) = 0$, $\theta_2 = \theta_1$. In this case, the flow properties remain unchanged.

To determine the position (x, y) of a node number i on the upper surface of coordinates (x_{E_i}, y_{E_i}), or the lower surface of coordinates (x_{I_j}, y_{I_j}) we choose a reference coordinate and a small step. The step can be constant or variable. Typically the reference coordinates is selected at the leading edge of the airfoil. By replacing the value of x_{E_i} in the airfoil equation, is easily to determine the value of its ordinate y_{E_i}. Similarly for the lower airfoil surface, there will y_{I_j} by the following relations:

$$x_{E_i} = \frac{(i-1)}{(k-1)} \quad \times C,\ y_{E_i} = f_E(x_{E_i})\ i = 1, 2, \ldots, k, \quad (15)$$

$$x_{I_j} = \frac{(j-1)}{(l-1)} \quad \times C,\ y_{I_j} = f_I(x_{I_j})\ j = 1, 2, \ldots, l, \quad (16)$$

For the determination of the angle deviation θ_i, made by a line segment connected between the points i and $i+1$ with the horizontal, in order to determine the flow angle deflection ψ, the following relationship is used:

$$\theta_i = arctg\left(\frac{y_{i+1} - y_i}{x_{i+1} - x_i}\right), \quad (17)$$

with: $i = 1, 2, \ldots, k$ for extrados, and $i = 1, 2, \ldots, l$ for intrados.

The region number 0 is the upstream infinity provided free data.

The flow in the region number 1 of the upper and the lower surface is given by the region number 0 of the upstream infinity.

The region number i of the upper or lower surface is limited by the nodes number i on the left and the node number $i+1$ on the right.

The pressures P_{Ei} and P_{Ij} are broken down into two components each one, as shown in Figure 4. The vertical component that represents the lift force is L_{Ei} of the upper, and L_{Ij} on the lower surface. Similarly, the horizontal components that represent the drag are D_{Ei} on the upper and D_{Ij} on the lower surface. The pitching moment of the two forces exerted on the extrados is named by m_{Ei} and the moment of the two forces exerted on the intrados is m_{Ij}. The pitching moment is calculated with respect to the point p, Figure 4. For the applications, $p = O$ is taken. Then, on the upper surface and per unit of depth we have

$$L_{E_i} = -P_{E_i} \times (x_{E_{i+1}} - x_{E_i}), \quad (18)$$

$$D_{E_i} = P_{E_i} \times (y_{E_{i+1}} - y_{E_i}), \quad (19)$$

$$m_{E_i} = -L_{E_i}\left(\frac{x_{E_{i+1}} + x_{E_i}}{2} - x_p\right) - D_{E_i}\left(\frac{y_{E_{i+1}} + y_{E_i}}{2} - y_p\right), \quad (20)$$

with $i = 1, 2, \ldots, k-1$

On the lower surface and per unit of depth we have

$$L_{I_j} = P_{I_j} \times (x_{I_{j+1}} - x_{I_j}), \quad (21)$$

$$D_{I_j} = -P_{I_j} \times (y_{I_{j+1}} - y_{I_j}), \quad (22)$$

$$m_{I_j} = L_{I_j}\left(\frac{x_{I_{j+1}} + x_{I_j}}{2} - x_p\right) + D_{I_j}\left(\frac{y_{I_{j+1}} + y_{I_j}}{2} - y_p\right), \quad (23)$$

with $j = 1, 2, \ldots, l-1$

The number of nodes k on the upper surface is not necessarily equal to the number of the nodes l on the upper surface. For applications, the leading edge is placed at the point O of the reference of calculation.

The total lift and drag across the airfoil are respectively considered as the sum of the forces on all segments (regions) of the upper and lower surfaces.

$$L = (L_{E_1} + L_{E_2} + \cdots + L_{E_k}) + (L_{I_1} + L_{I_2} + \cdots + L_{I_l}), \tag{24}$$

$$D = (D_{E_1} + D_{E_2} + \cdots + D_{E_k}) + (D_{I_1} + D_{I_2} + \cdots + D_{I_l}), \tag{25}$$

$$m = (m_{E_1} + m_{E_2} + \cdots + m_{E_k}) + (m_{I_1} + m_{I_2} + \cdots + m_{I_l}). \tag{26}$$

The pitching moment is considered positive when it rotates counter clockwise, Figure 4.

The aerodynamic coefficients are obtained as follows:

$$C_L = \frac{L}{q_0 \times S}, \tag{27}$$

$$C_D = \frac{D}{q_0 \times S}, \tag{28}$$

$$C_m = \frac{m}{q_0 \times S \times C}, \tag{29}$$

where

$$q_0 = \frac{1}{2}\gamma(T_0)P_0M_0^2. \tag{30}$$

The surface of reference S is considered to be the airfoil chord per unit of depth.

By varying the parameters M_0, t/C, α and T_0 as well as the airfoil shape, it is possible to find all the possible parameters and in particular the effect of T_0 when it is high. A comparison between the PG model and the HT model is performed.

4 Applications

Our applications are limited by three types of airfoils which are symmetrical lozenge, Symmetrical curved airfoil and unsymmetrical curved airfoil. The calculation of the pitching moment is made to the leading edge.

4.1 Symmetrical lozenge

The lozenge is shown in Figure 5. We can meet this type of airfoil for building applications wings of supersonic aircraft. The geometry is given by the maximum thickness t. It is chosen in the middle of the chord. With $0 \leq x/C \leq 1$.

We discretize the airfoil into $k = l = 3$ nodes. Two regions in upper and lower surface will be sufficient to describe the flow and to have the exact solution.

4.2 Symmetrical curved airfoil

The form of this type of airfoil is shown in Figure 6. The equation of the extrados and the intrados is chosen as a polynomial of 3rd degree. Its equation is given by:

Fig. 5. Symmetrical lozenge

Fig. 6. Symmetrical curved airfoil.

Fig. 7. Curved non symetrical airfoil.

$$f_E(x) = -f_I(x) = \frac{27}{8}t\frac{x}{C}\left(1 - \frac{x}{C}\right)^2, \tag{31}$$

where $0 \leq x/C \leq 1$. The maximum thickness t of this airfoil is at a distance $x/C = 1/3$ from the leading edge.

4.3 Curved non symetrical airfoil

The shape of the upwards curved airfoil is shown in Figure 7. The upper and lower surface are selected from the parabolic equation witch respect 3 chosen conditions. We encountered this type of airfoil applications for blade of compressor. The equation of the extrados and the intrados are respectively chosen by:

$$\frac{f_E(x)}{t_E} = \frac{f_I(x)}{t_E - t} = 4\frac{x}{C}\left(1 - \frac{x}{C}\right). \tag{32}$$

With $0 \leq x/C \leq 1$. In this case, the maximum thickness t of this airfoil lies in the middle of the chord. This type of airfoil is referred to as a skeletal airfoil. The value of t_E is chosen arbitrarily greater than 0. While $t/C = 0.03$ for the applications.

5 Error of *PG* model compared to *HT* model

For each parameter, the error given by the PG model compared to our HT model can be calculated by the following relation, for aim to compare the two models:

$$\varepsilon_{\text{Parameter}}(\%) = |1 - \frac{\text{Parameter}_{PG}}{\text{Parameter}_{HT}}| \times 100. \tag{33}$$

6 Results and comments

The results were divided into eight parts. In order to obtain graphical results, we have used a discretization of $k = l = 1000$ points on the extrados and on the intrados. For the tabulated results, we have used a discretization of $k = l = 8000$ points. This discretization is chosen in such a way that there will be 5 exact digits of the solution. Figures 9–21 contain four curves. Curves 1–4 respectively represent the variation of the parameter at HT for $T_0 = 3000\,\text{K}$, $T_0 = 2000\,\text{K}$, $T_0 = 1000\,\text{K}$

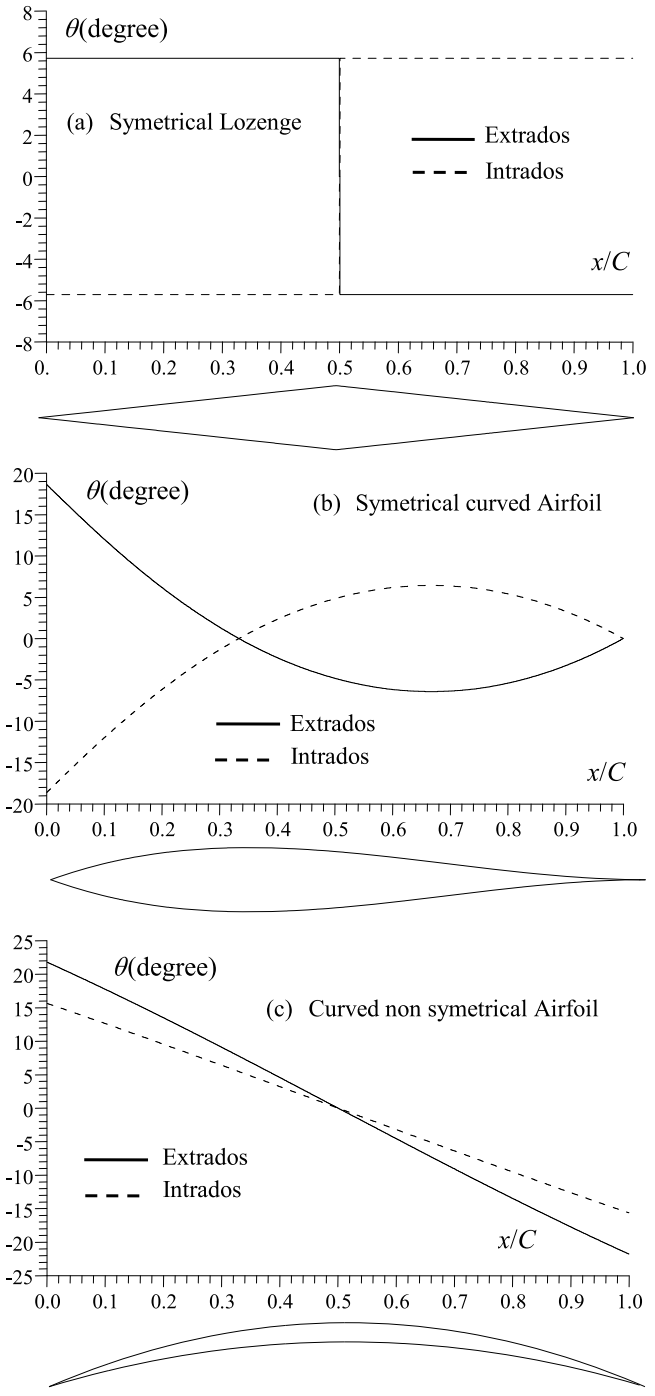

Fig. 8. Variation of the flow angle deviation along the extrados and the intrados of the selected airfoils.

and the case PG for $\gamma = 1.402$. Figure 9–12 contain 8 curves. 4 curves in continuous line are to represent the variation of the selected parameter on the extrados of the airfoil with HT. The 4 dashed curves represent the variation of the selected parameter on the airfoil intrados.

In this study three airfoils have been considered as Figures 5–7 shown them. The third airfoil (Fig. 7) is characterized by two parameters. While the 1st and 2nd airfoils are characterized by one parameter. One can even consider airfoils with several parameters.

The results for the PG model can be found in references [17]. They are presented for comparison with the HT model.

6.1 Typical example

In this example, we chose three very interesting airfoils in aerodynamics. The aim is to present the effect of T_0 on C_D, C_L, C_m and ΔS_{21} in a numerical way as well as the calculation of the error committed by the PG model with respect to the HT model for each value of T_0.

Table 1 shows the effect of T_0 on C_D, C_L, C_m and ΔS_{21} for the symmetrical lozenge of Figure 5 when $\alpha = 2.0\,°$, $M_0 = 4.00$ and $t/C = 0.1$, followed by the given errors of PG model on these coefficients with respect to the HT model as represented in Table 2.

Table 3 shows the effect of T_0 on C_D, C_L, C_m and ΔS_{21} for the symmetric curved airfoil of Figure 6 when $\alpha = 2.0\,°$, $M_0 = 4.00$ and $t/C = 0.1$, followed by the given errors of PG model on these coefficients with respect to HT model as represented by Table 4.

Table 5 shows the effect of T_0 on C_D, C_L, C_m and ΔS_{21} for the non-symmetric curved airfoil of Figure 7 when $\alpha = 2.0\,°$, $M_0 = 4.00$ and $t/C = 0.2$, followed by the given errors of PG Model on these coefficients with respect to HT model as represented by Table 6. For this third airfoil, $t_E/C = 0.03$ was taken for the application.

We clearly notice the T_0 effect on all aerodynamic parameters for the selected three airfoils. The difference between the PG and HT models increases with increasing of T_0. The maximum error is noticed on the coefficient C_L which can arrive at 35% when $T_0 = 3000\,\mathrm{K}$ and which can arrive at 39.38% when $T_0 = 3500\,\mathrm{K}$ for $M_0 = 4.00$ and $\alpha = 2.00$. It is noted that the shape of the airfoil also influences the difference between the two models, although the parameters α, M_0 and t/C are the same for the three airfoils. The PG model determines the aerodynamic parameters with excess. It is designed to solve low T_0 problems. Then, if T_0 increases, the performance of the flow will be degraded with respect to the PG model.

6.2 Variation of the flow deviation along airfoil surface

Figure 8 shows the variation in the deviation of the airfoil wall which also represents the variation of the flow deviation along the surface of the selected three airfoils. This deviation enters into the calculation of the value of ψ determining the type of the flow, whether compression or expansion, given by this deviation.

6.3 Variation of the parameters along the airfoil surface

Figures 9–12 show the effect of T_0 on the variation of M, T/T_0, ρ/ρ_0 and P/P_0 along the surface of the extrados and the intrados of the three selected airfoils. In Figures 11 and 12 the ratios ρ/ρ_0 and P/P_0 are calculated with respect to the total local conditions of the segments. We clearly notice the effect of T_0 on all thermodynamic parameters with a degradation of M and T/T_0 when T_0 decrease, and increase

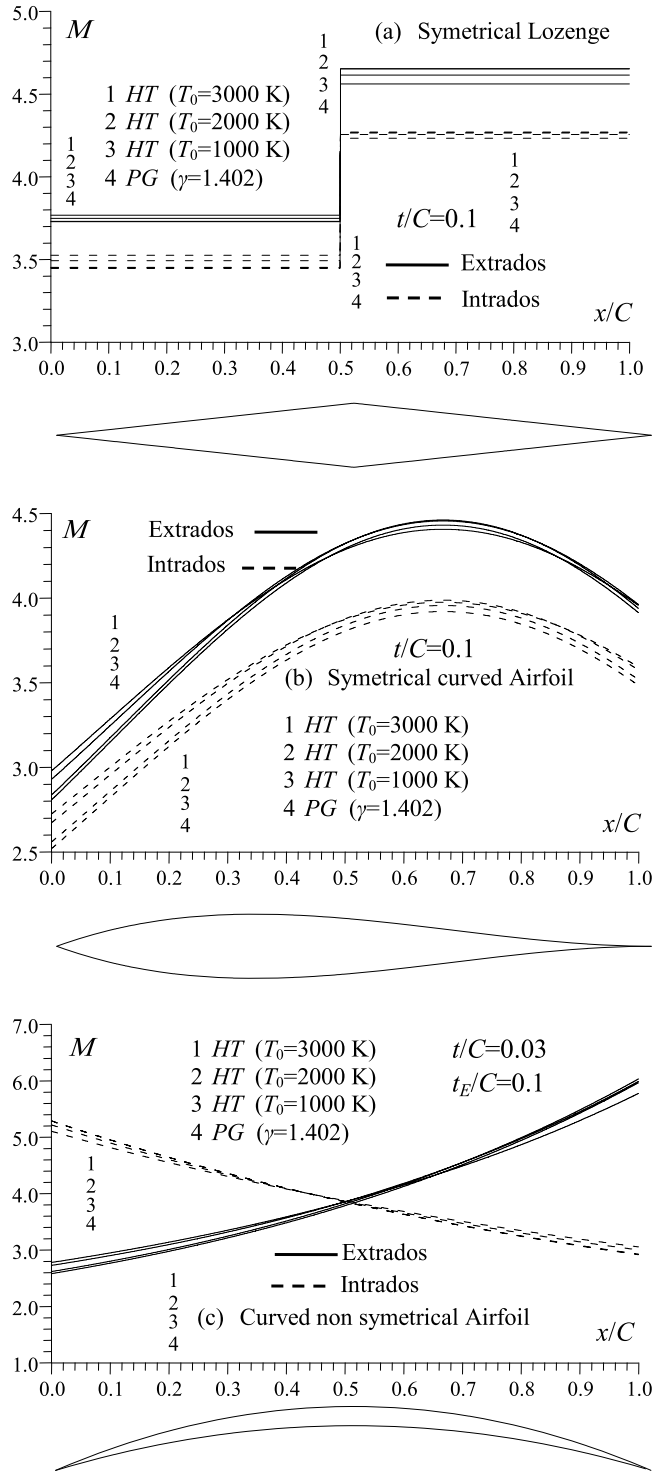

Fig. 9. Effect of T_0 on the variation of M along the surface of the three selected airfoils when $\alpha = 2.0\,^\circ$ and $M_0 = 4.00$.

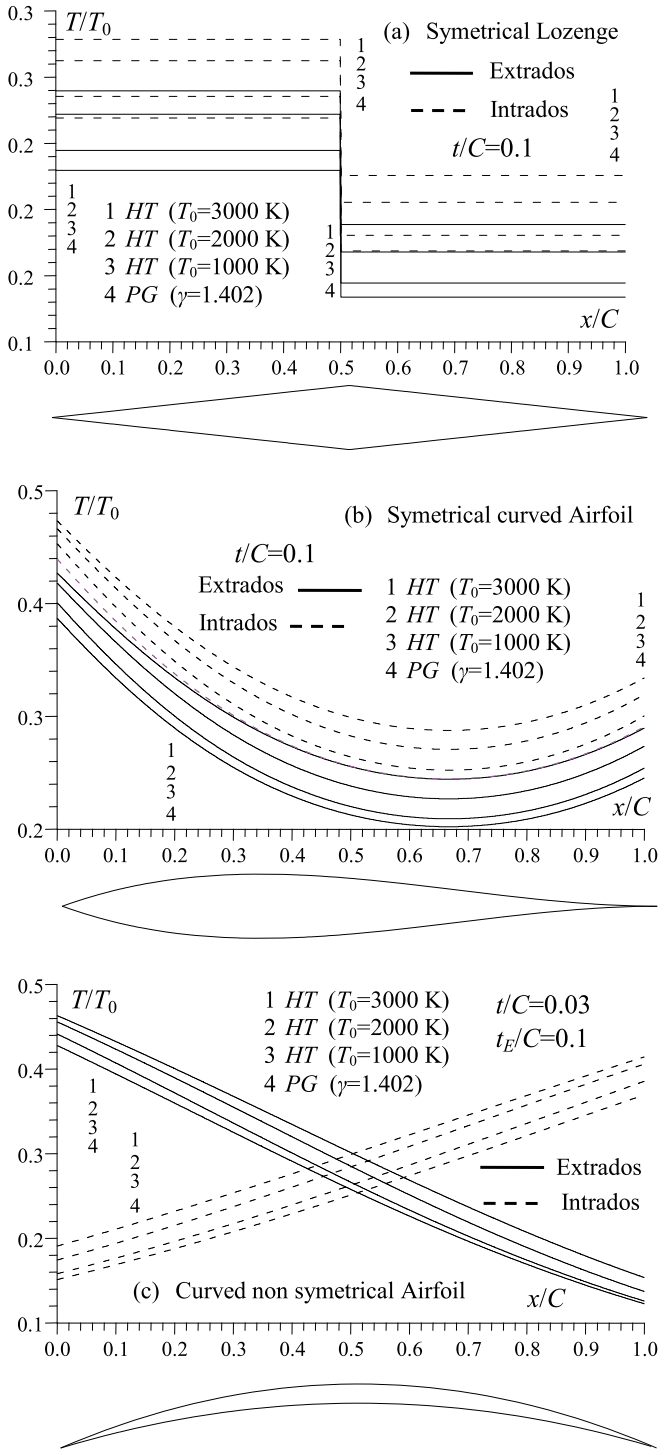

Fig. 10. Effect of T_0 on the variation of T/T_0 along the surface of the three selected airfoils when $\alpha = 2.0\,^\circ$ and $M_0 = 4.00$.

of ρ/ρ_0 and P/P_0 when T_0 increases gradually. This influence necessarily gives the influence of T_0 on all the aerodynamic coefficients C_D, C_L and C_m.

The variation of these parameters is related to the deviation of the wall, shown in Figure 8, along the airfoil surface. As the wall deviation takes two values on the extrados and on the intrados of lozenge, one will consequently have 2 values of these parameters on the extrados and on the intrados. While for the other two airfoils there is a continuous variation along the surface of the airfoils. Thus the airfoil shape, in addition to T_0, affects the variation of the parameters on the airfoil surface.

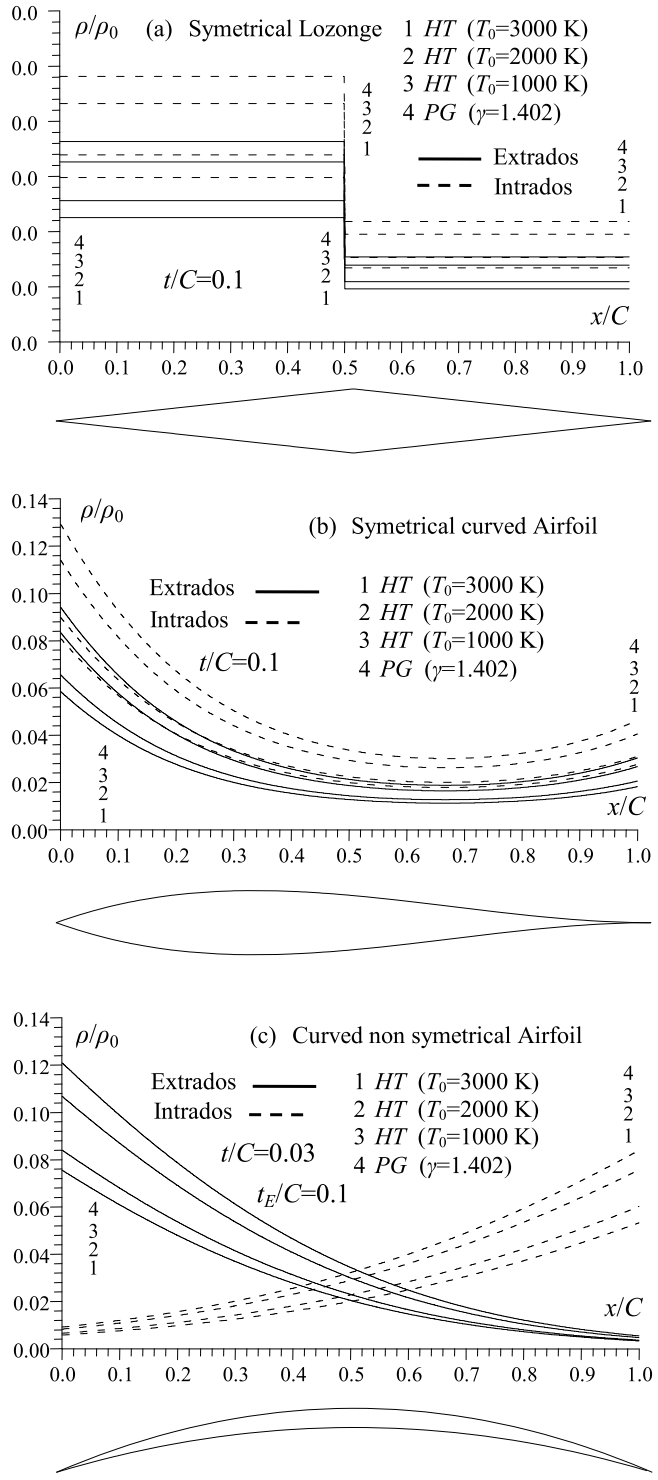

Fig. 11. Effect of T_0 on the variation of ρ/ρ_0 along the surface of the three selected airfoils when $\alpha = 2.0°$ and $M_0 = 4.00$.

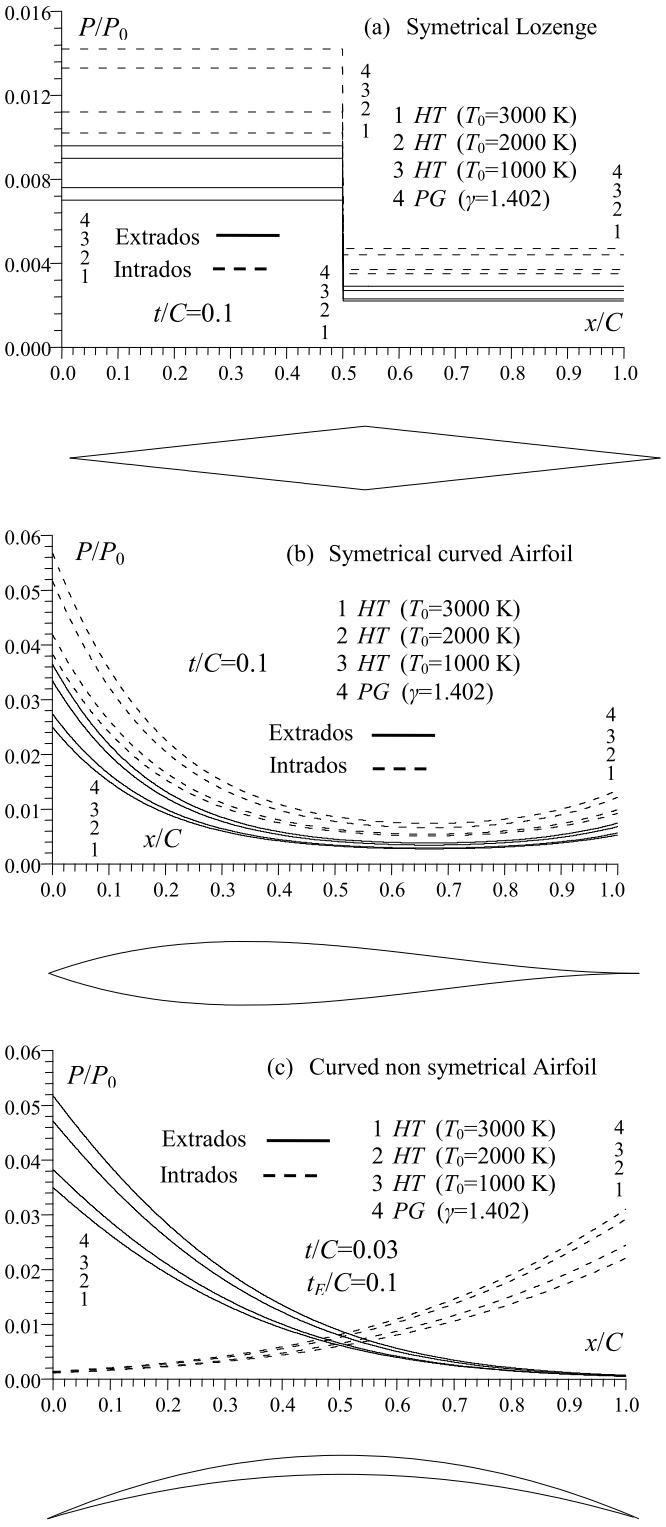

Fig. 12. Effect of T_0 on the variation of P/P_0 along the surface of the three selected airfoils when $\alpha = 2.0°$ and $M_0 = 4.00$.

6.4 Effect of α to HT on the aerodynamic coefficients for fixed M_0 and t/C

Figures 13–15 represent the effect of T_0 respectively on the variation of C_D, C_L and C_m as a function of α for the three airfoils when $M_0 = 4.00$. For the symmetrical airfoils, we have found a symmetry of the variation of C_D, C_L and C_m. While for the third airfoil, this symmetry is not present, since the airfoil is not symmetrical. We clearly notice the effect of T_0 on the three parameters. To determine the actual value of C_D, C_L and C_m, the value obtained from Figures 13–15 must be divided by 10^3.

Table 1. Effect of T_0 on C_D, C_L, C_m and $\Delta S_{21}/R$ for the lozenge when $\alpha = 2.0°$, $M_0 = 4.00$ and $t/C = 0.1$.

	PG	*HT* T_0 (K)		
	$\gamma = 1.402$	1000	2000	3000
C_D (10^3)	0.07047	0.06961	0.06015	0.05489
C_L (10^3)	0.25847	0.25451	0.21908	0.19981
C_m (10^3)	0.10140	0.09980	0.08620	0.07895
$\Delta S_{21}/R$	0.04326	0.03848	0.03459	0.03541

Table 2. Error of *PG* model compared to *HT* model according to Table 1.

$\varepsilon(\%)$	$T_0 = 1000$ K	$T_0 = 2000$ K	$T_0 = 3000$ K
$\varepsilon(C_D)$	1.23	17.15	28.38
$\varepsilon(C_L)$	1.55	17.97	29.35
$\varepsilon(C_m)$	1.60	17.63	28.43

Table 3. Effect of T_0 on C_D, C_L, C_m and $\Delta S_{21}/R$ for the symmetrical curved airfoil when $\alpha = 2.0°$, $M_0 = 4.00$ and $t/C = 0.1$.

	PG	*HT* T_0 (K)		
	$\gamma = 1.402$	1000	2000	3000
C_D (10^3)	0.14376	0.14138	0.12087	0.10980
C_L (10^3)	0.27933	0.27055	0.22723	0.20630
C_m (10^3)	0.10603	0.10236	0.08608	0.07844
$\Delta S_{21}/R$	0.73606	0.68655	0.64513	0.66500

Table 4. Error of *PG* model compared to *HT* model according to Table 3.

$\varepsilon(\%)$	$T_0 = 1000$ K	$T_0 = 2000$ K	$T_0 = 3000$ K
$\varepsilon(C_D)$	1.68	18.93	30.92
$\varepsilon(C_L)$	3.24	22.92	35.40
$\varepsilon(C_m)$	3.58	23.17	35.17

Table 5. Effect of T_0 on C_D, C_L, C_m and $\Delta S_{21}/R$ for the non-symmetrical curved airfoil when $\alpha = 2.0°$, $M_0 = 4.00$ and $t/C = 0.03$ and $t_E/C = 0.2$.

	PG	*HT* T_0 (K)		
	$\gamma = 1.402$	1000	2000	3000
C_D (10^3)	1.85497	1.81198	1.52967	1.38558
C_L (10^3)	0.20469	0.23986	0.26185	0.25586
C_m (10^3)	1.23532	1.22749	1.06738	0.97667
$\Delta S_{21}/R$	1.41865	1.37919	1.36966	1.39133

In Figures 13–15, the range of variation of the incidence angle α is taken $[-10°, 10°]$. Generally beyond this interval, we will have the phenomenon of stall.

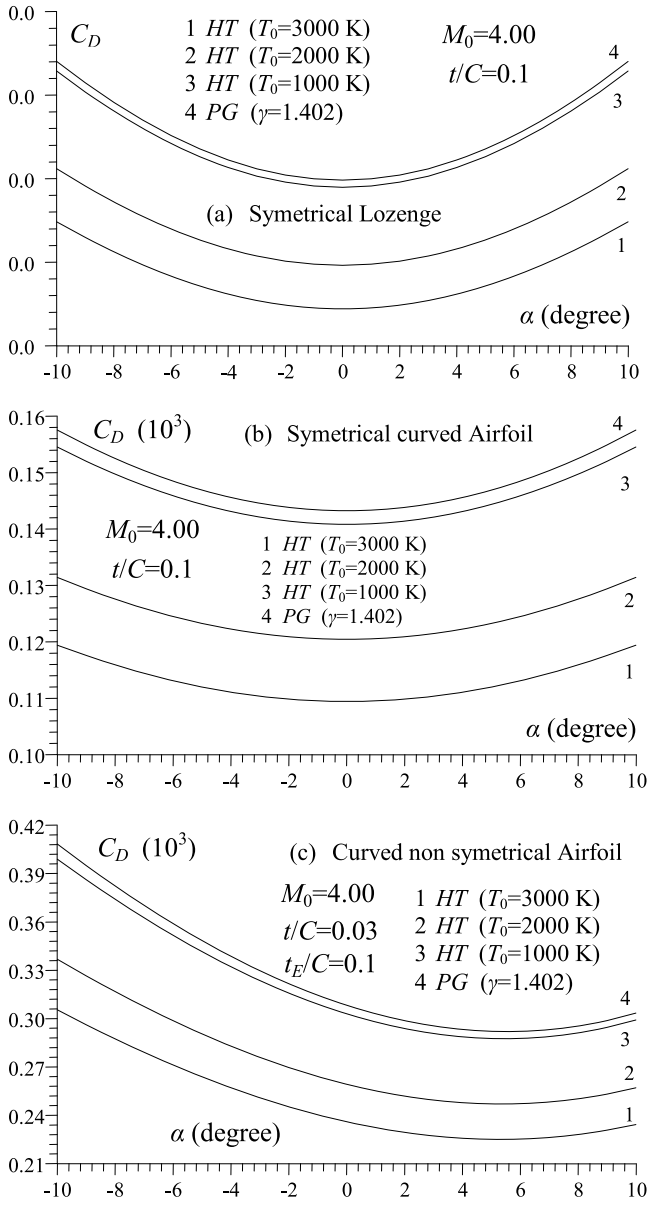

Fig. 13. Effect of T_0 on the variation of C_D as a function of α.

It is very important to determine an angle of incidence which makes it possible to find $C_L = 0$, called angle of zero lift, and the incidence angle making it possible to find $C_m = 0$, called zero moment angle. For symmetrical airfoils, this angle is equal to 0.0. Whereas for the non-symmetric airfoils, force will have a value other than zero and which depends on T_0. Table 7 shows the effect of T_0 on the zero lift angle for the third non-symmetric airfoil and Table 8 shows the effect of T_0 on the zero moment angle for the third airfoil for some values of M_0 when $t/C = 0.03$ and $t_E/C = 0.1$. We notice the effect of T_0, M_0, t/C, the shape of airfoil and t_E/C on these two remarkable angles.

It is clear that for an incidence angle α in the vicinity of the angle of zero lift, or the angle of zero moment, of one degree, there is no influence of T_0 on these parameters.

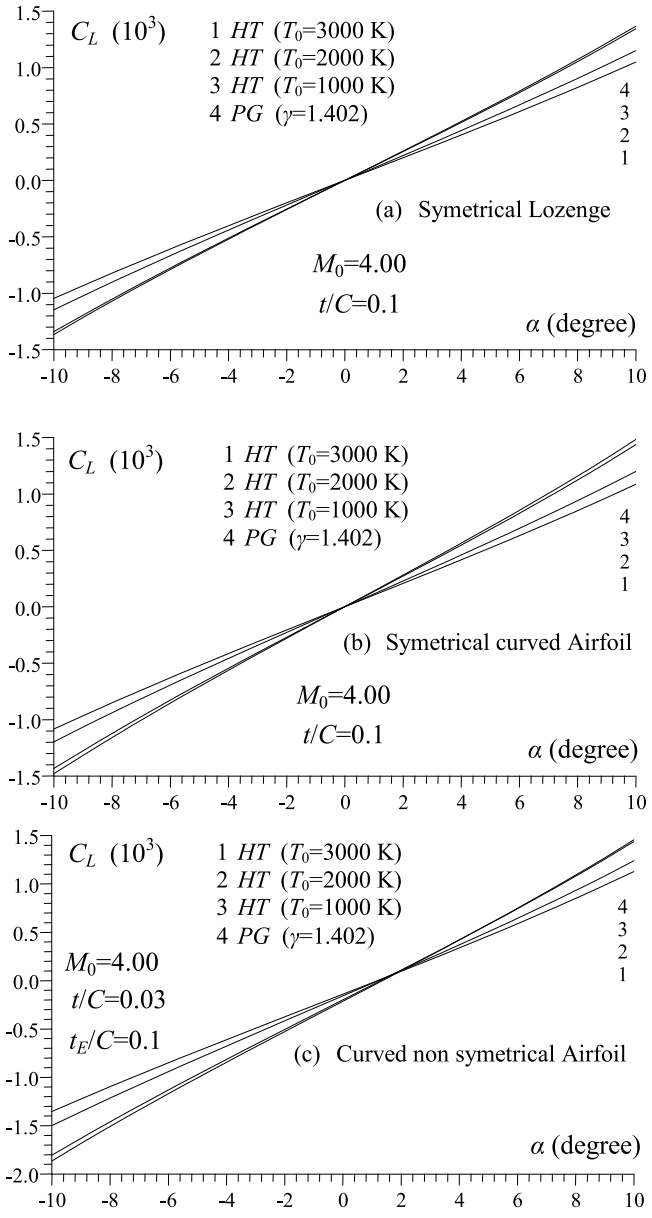

Fig. 14. Effect of T_0 on the variation of C_L as a function of α.

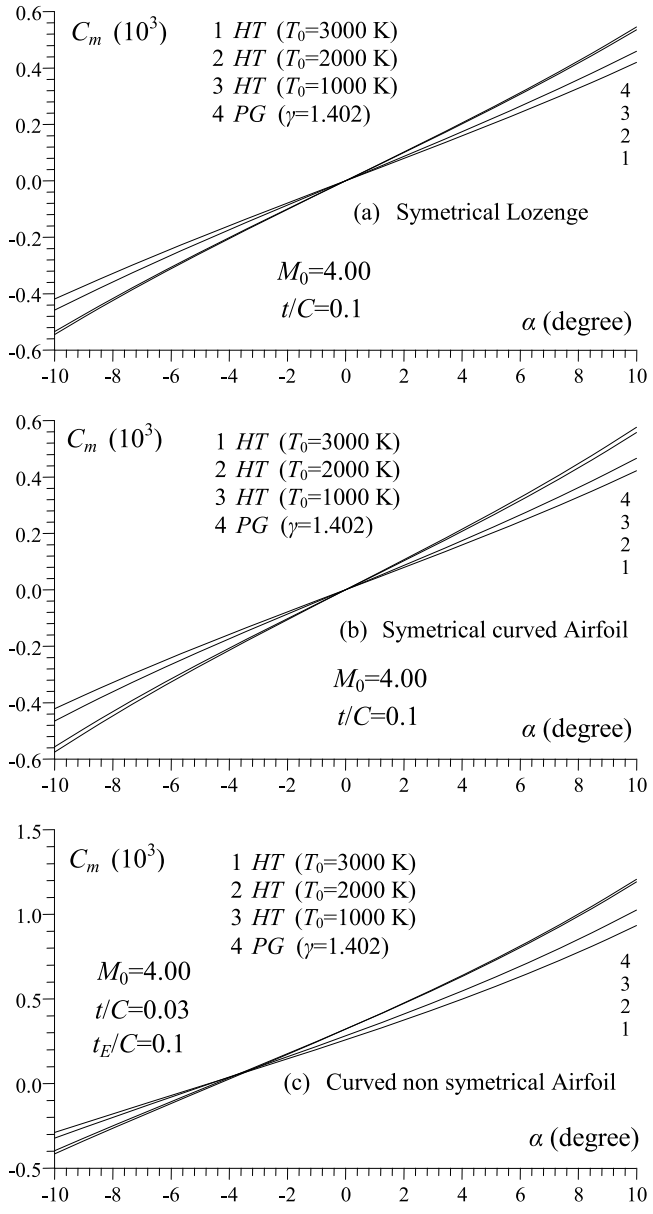

Fig. 15. Effect of T_0 on the variation of C_m as a function of α.

Table 6. Error of *PG* model compared to *HT* model according to Table 5.

$\varepsilon(\%)$	$T_0 = 1000$ K	$T_0 = 2000$ K	$T_0 = 3000$ K
$\varepsilon(C_D)$	2.31	17.53	25.30
$\varepsilon(C_L)$	17.18	27.92	33.56
$\varepsilon(C_m)$	0.63	13.59	22.93

Table 7. Effect of T_0 the zero lift angle for the third non-symmetric airfoil in function of M_0.

	PG	*HT* T_0 (K)		
M_0	$\gamma = 1.402$	1000	2000	3000
2.00	1.12621	1.06831	1.00951	0.98844
3.00	1.22893	1.16998	1.10840	1.08275
4.00	1.36949	1.30556	1.21869	1.19970
5.00	1.44686	1.38326	1.26308	1.24281

6.5 Effect of M_0 at *HT* on the aerodynamic coefficients for fixed α and t/C

Figures 16–18 represent the effect of T_0 respectively on the variation of the aerodynamic coefficients C_D, C_L and C_m as a function of M_0 for the three selected airfoils when $\alpha = 2.0\,°$C. The presentation is done on a Logarithmic scale because of the fact that the small values are grouped in a Figure with the large values of the aerodynamic coefficients. We clearly notice the effect of T_0 on these

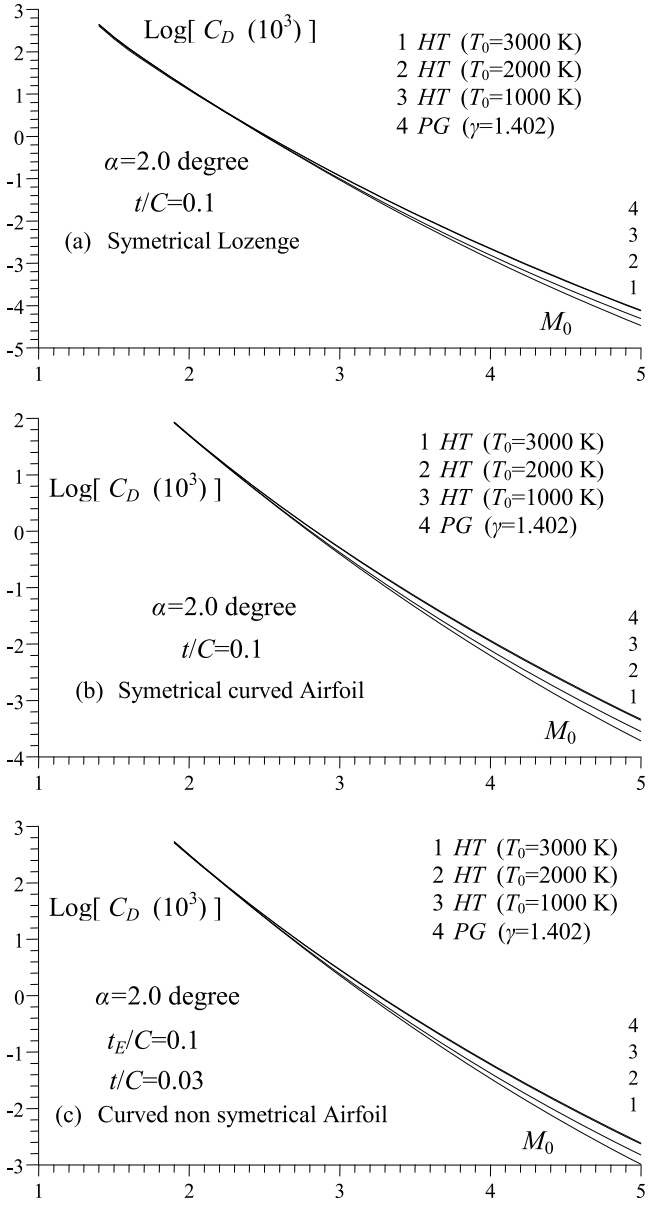

Fig. 16. Effect of T_0 on the variation of C_D as a function of M_0.

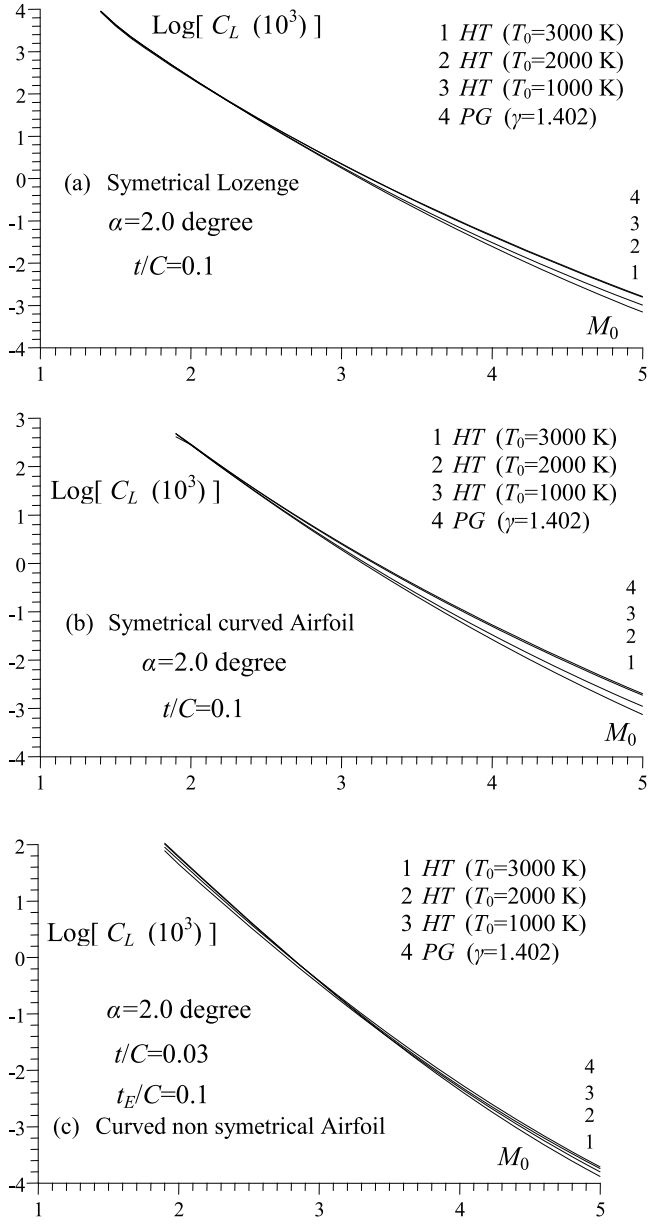

Fig. 17. Effect of T_0 on the variation of C_L as a function of M_0.

Table 8. Effect of T_0 the zero moment angle for the non-symmetric airfoil in function of M_0.

	PG	*HT* T_0 (K)		
M_0	$\gamma = 1.402$	1000	2000	3000
2.00	/	/	/	/
3.00	−4.62572	−4.72499	−4.84051	−4.89225
4.00	−4.37190	−4.47564	−4.63459	−4.67646
5.00	−4.12962	−4.22671	−4.43716	−4.47744

coefficients. This effect becomes important as M_0 increases gradually. Then for small values of M_0 up to about $M_0 < 2.00$, the difference between the *PG* and *HT* models is not significant, which shows that the results given by the *PG* model are acceptable. But if M_0 increases, independently of T_0, the corrections made by the *HT* model are necessary, which shows the interest of the *HT* model for the large values of $M_0 > 2.00$. Generally this limit depends on the error considered in the calculation. It should also be noted that if M_0 decreases, there will be the appearance of a detached shock wave which develops at the leading edge of the airfoil. Commentaries remain valid for any values of α, t/C and t_E/C.

The variation of M_0 in Figures 16–18 starts from $M_{0_{min}}$ up to 5.0. We note the effect of T_0 on the minimum value of the Mach number upstream $M_{0_{min}}$, that can have the flow to limit the attached shock with the detached shock, respectively for the three selected airfoils. Forcing this limit depends on T_0, α, t/C and t_E/C. The limit given by the *PG* model $M_{0_{min}}(PG) > M_{0_{min}}(HT)$ is considered as an attached shock for the *HT* model, since, that is to say one can have a Mach

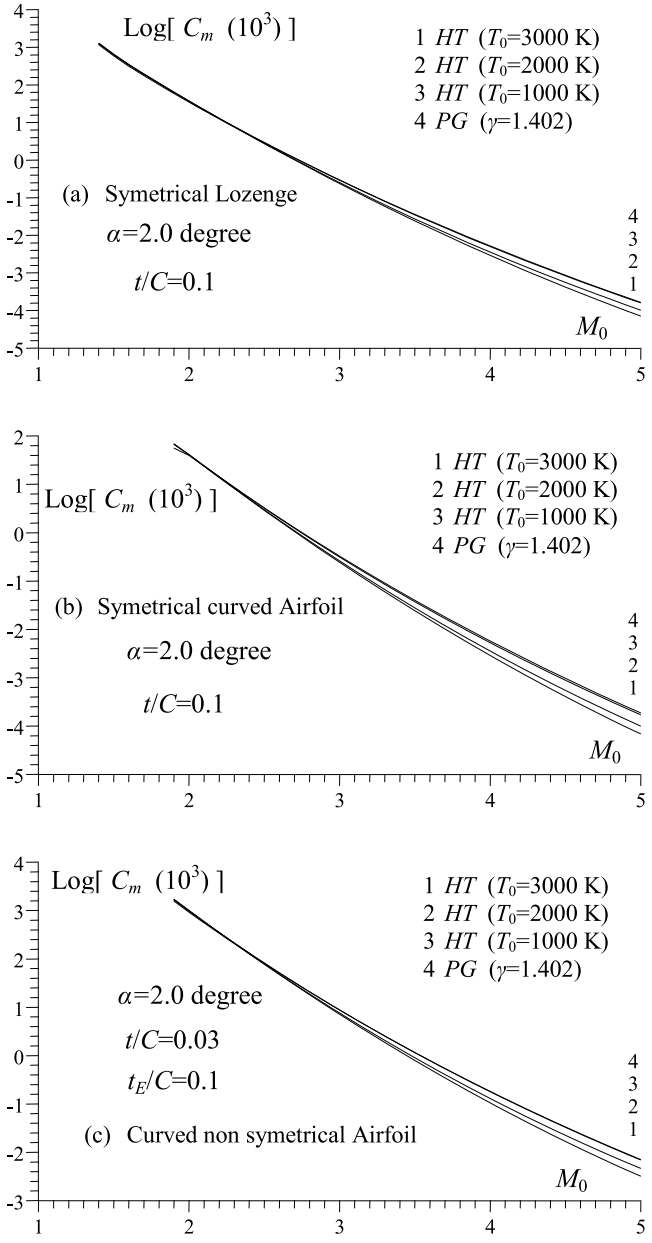

Fig. 18. Effect of T_0 on the variation of C_m as a function of M_0.

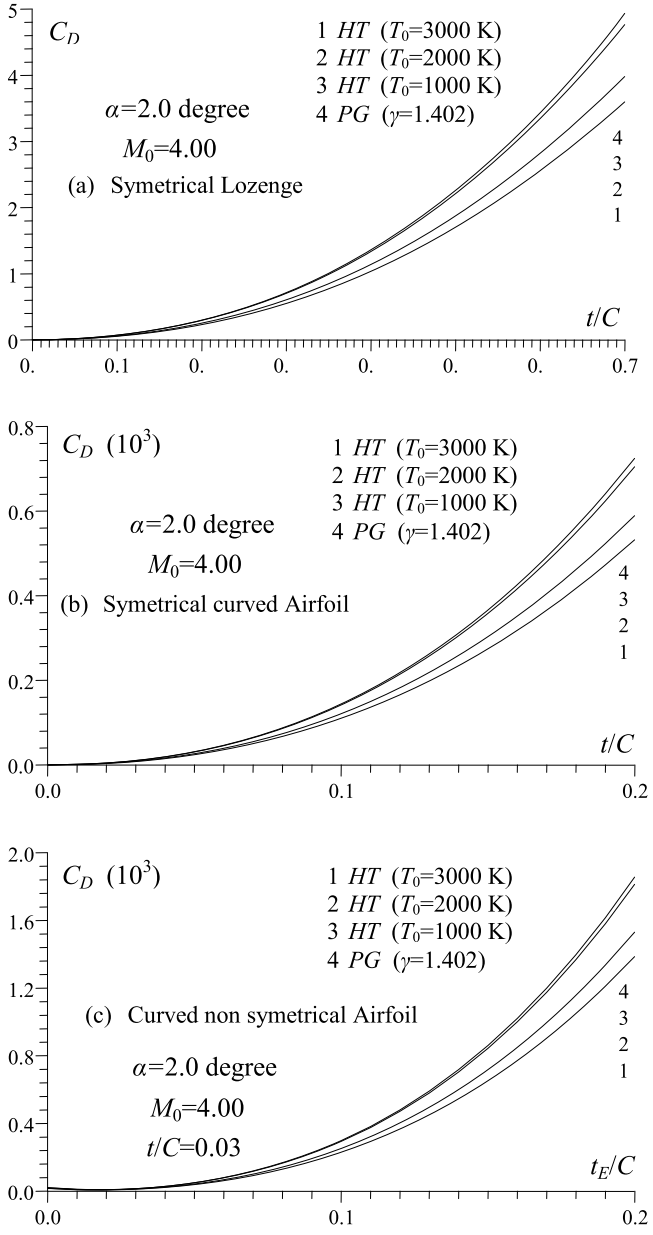

Fig. 19. Effect of T_0 on the variation of C_D as a function of t/C.

number $M_0 < M_{0_{min}}(PG)$ for HT with the possibility of finding an attached shock. It is noted that the margin of finding a detached shock is greater for the third non-symmetric airfoil than the two other. Then $M_{0_{min}}$ not only depends on α, t/C, but also depends on the shape of the airfoil.

6.6 Effect of t/C at HT on the aerodynamic coefficients for fixed M_0 and α.

Figures 19–21 represent the effect of T_0 respectively on the variation of C_D, C_L and C_m as a function of the thickness t/C of the three airfoils when $M_0 = 4.00$ and $\alpha = 2.00$. For the non-symmetrical airfoil, the curvature of the extrados was varied without touching the airfoil thickness taken at $t/C = 0.03$. We note the effect of T_0 on these parameters, despite the small thickness, which requires the use of the HT model for corrections despite at low t/C. It is also noted that if T_0 decreases, the HT model becomes non-comparable with the PG model. Then when $T_0 < 240$ K, the PG model gives acceptable results. It should also be noted that the shape of the airfoil will still influences the variation of these coefficients.

It is noted that if t/C increases, it will be possible to find a detached shock. If $t/C \leq (t/C)_{\max}$, there will necessarily be an attached shock, hence a solution can be given by the developed program. If $t/C > (t/C)_{\max}$, we will have the appearance of a detached shock wave.

6.7 Variation of the aerodynamic coefficients as a function of T_0 for fixed α, M_0 and t/C

Figures 22–24 represent the variation of the aerodynamic coefficients of the three selected airfoils as a function of T_0

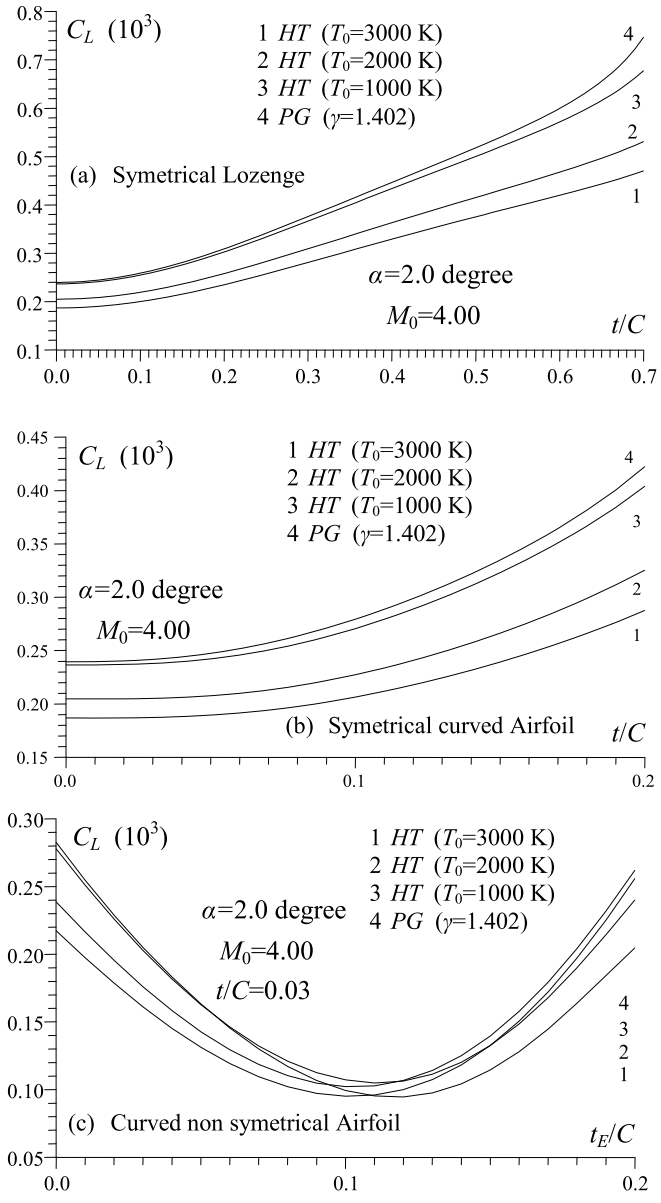

Fig. 20. Effect of T_0 on the variation of C_L versus t/C.

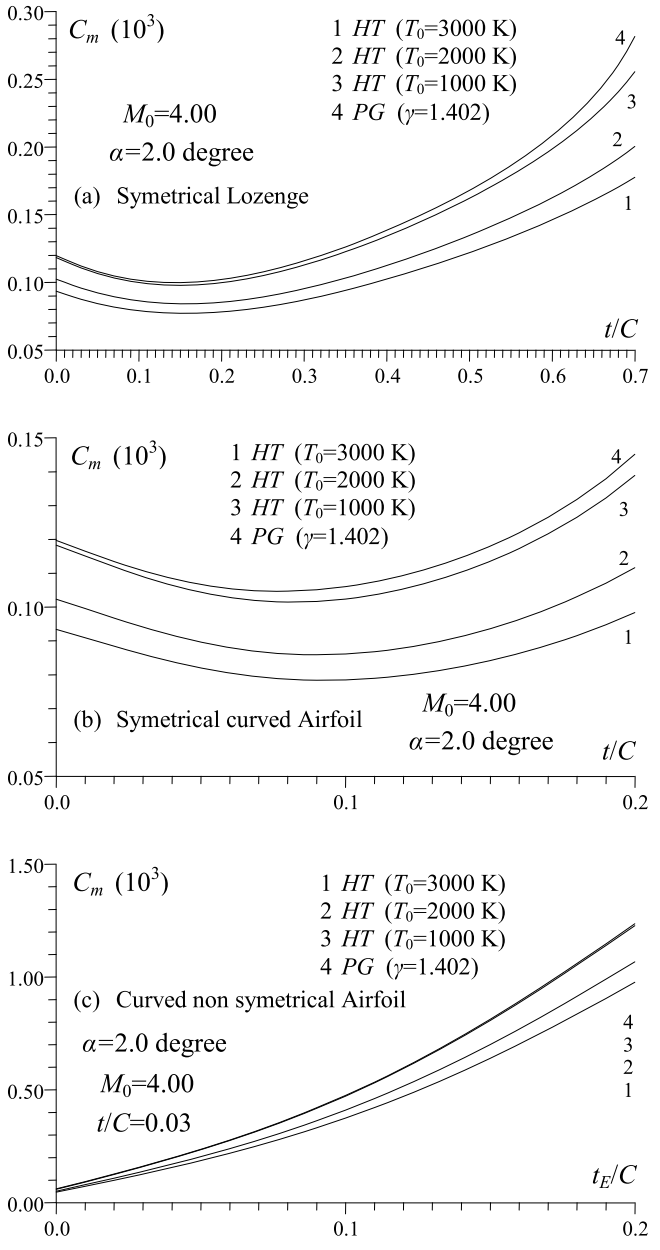

Fig. 21. Effect of T_0 on the variation of C_m versus t/C.

and the comparison with the *PG* model. The latter does not depend on T_0, where it is represented by a horizontal straight line along the entire interval. The C_D, C_L and C_m variation is chosen for $M_0 = 4.00$ and $\alpha = 2.00°$. We can note the effect of T_0 on these parameters. Hence the need to use the *HT* model for possible corrections. One notices again when T_0 is small, the *HT* model becomes confounded with the *PG* model. We can go to about 240 K. Then when $T_0 < 240$ K, the *PG* model gives acceptable results. It is also noted that the shape of the airfoil still influences the variation of these coefficients since the variation of the aerodynamic coefficients of the three airfoils is not the same. We note that the *HT* model degrades the C_D, C_L and C_m values due to their decrease with increasing of T_0, which does not work with the physical and real behavior of the flow.

6.8 Variation of the error caused by the *PG* model compared to *HT* model as a function of M_0

Figures 25–27 represent the variation of the relative error caused by the use of the *PG* model with respect to the *HT* model on the aerodynamic coefficients C_D, C_L and C_m of the three selected airfoils. The application is made for the temperatures $T_0 = 1000$ K, 2000 K and 3000 K and for $\alpha = 2.00°$ and $t/C = 0.1$. It can be seen that the error increases considerably and can reach 55% when $T_0 = 3000$ K and $M_0 = 5.00$. This error is noticed for the coefficients C_L and C_m for the symmetrical curved airfoil. This value also increases with the airfoil shape, t/C and α. This value of the maximum error give the obligation to use

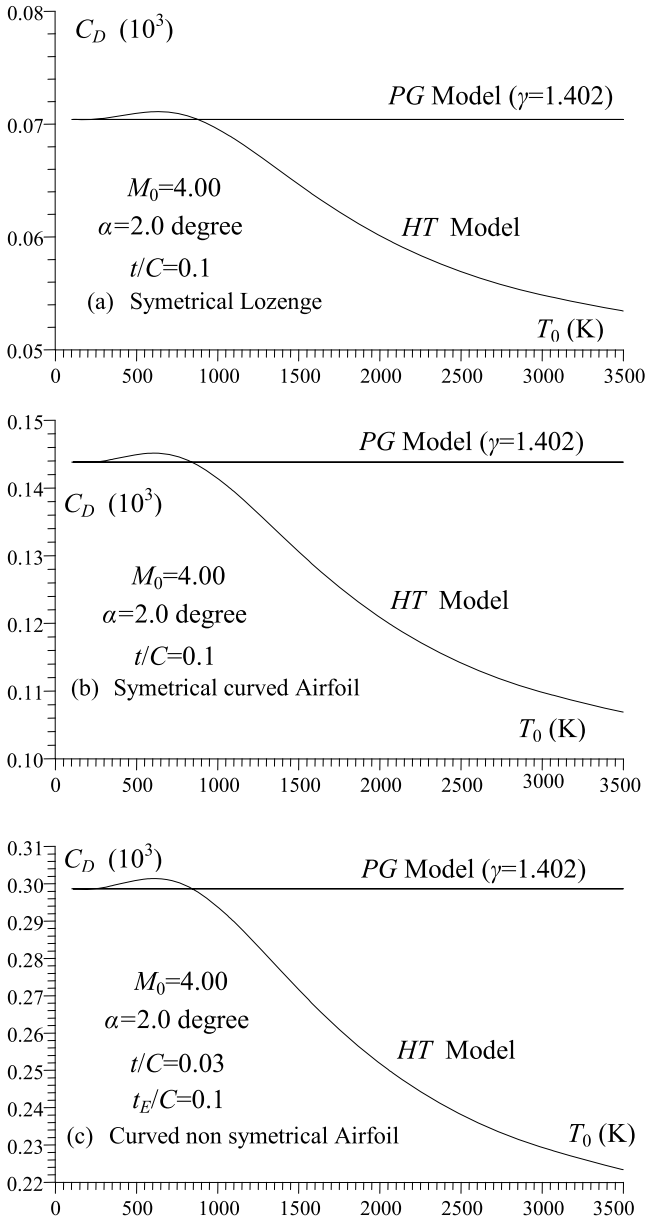

Fig. 22. Variation of C_D as a function of T_0.

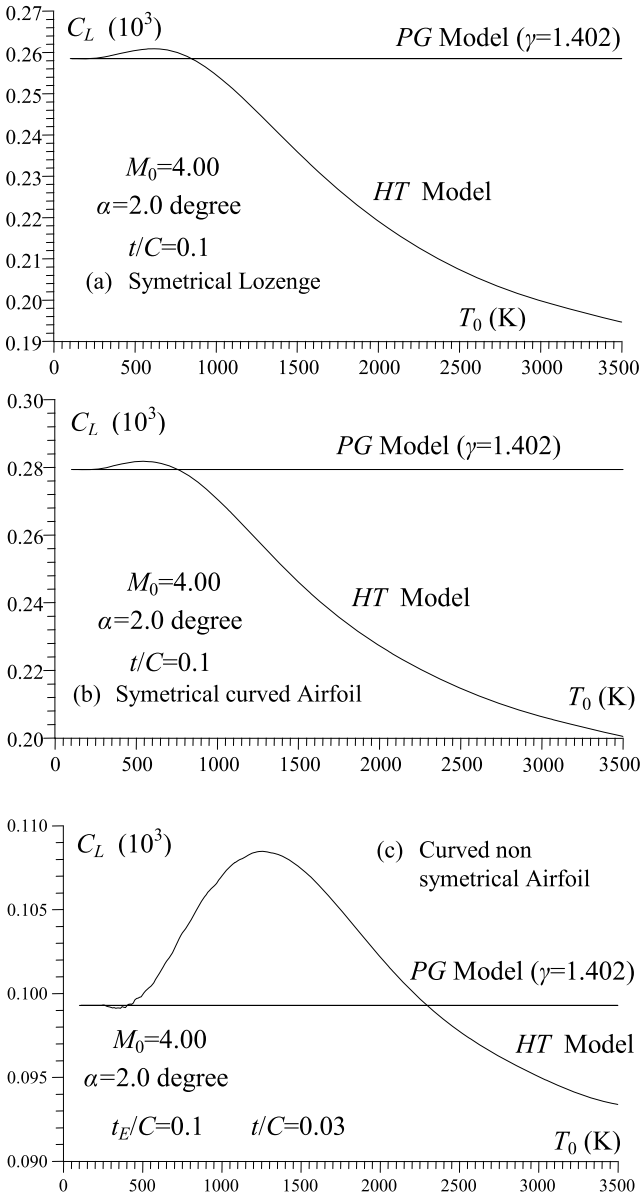

Fig. 23. Variation of C_L as a function of T_0.

the HT model for possible corrections to the results given by the PG model when T_0 is high and begins to exceed the 240 K approximately.

7 Conclusion

The conclusions that can be deducted are:

A detached shock occurs for lower M_0.

Detached shock still occurs when the angle ψ exceeds a certain maximum angle.

The computational accuracy for the PG and HT models depends on the discretization, which results in the choice of k and l for the curved shapes. More k and l will be high, we will have a good accuracy.

The PG model gives acceptable results for small values of $M_0 < 2.00$, $T_0 < 240$ K and $t/C < 1.0$ approximately. On the other hand, when M_0 or T_0 or t/C increases, the PG model gives results which are different from the real case, hence the need for the HT model.

The developed numerical program can process any gas found in nature. In this case, we must add the variation of the specific heat $C_P(T)$ and the constant R of the gas with the calculation of $H(T)$.

The convergence of the results requires an additional calculation time for the HT model compared to the PG model for the same accuracy.

A condensation of the nodes in the Simpson quadrature is used to integrate the function with high precision in a reduced time.

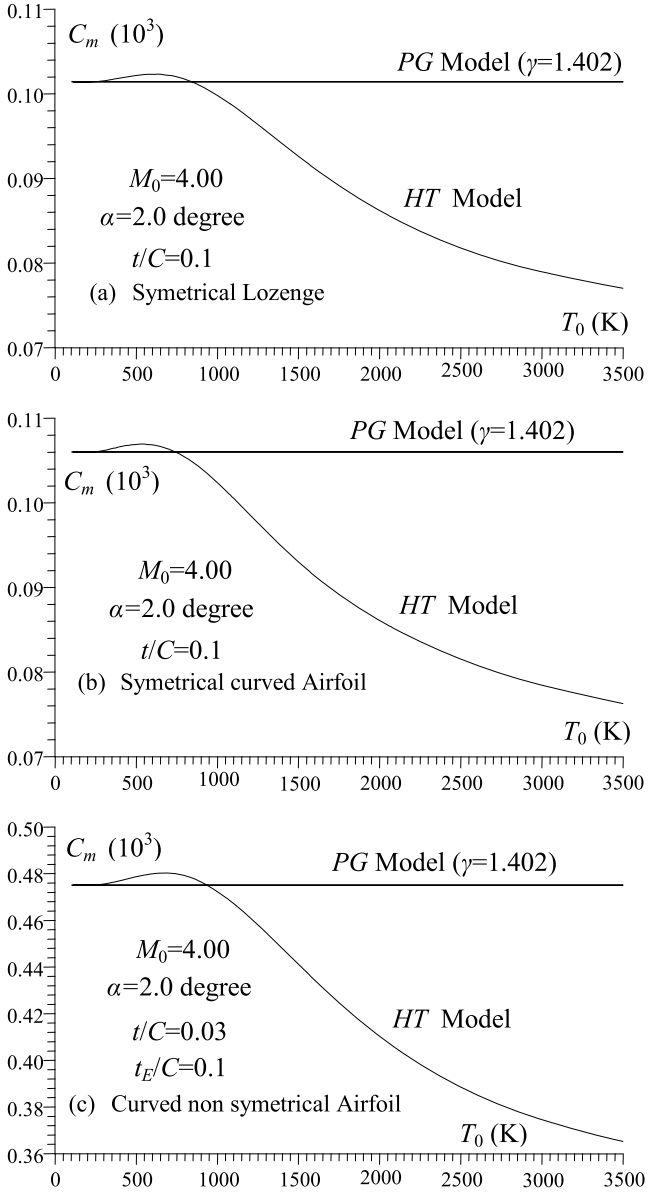

Fig. 24. Variation of C_m as a function of T_0.

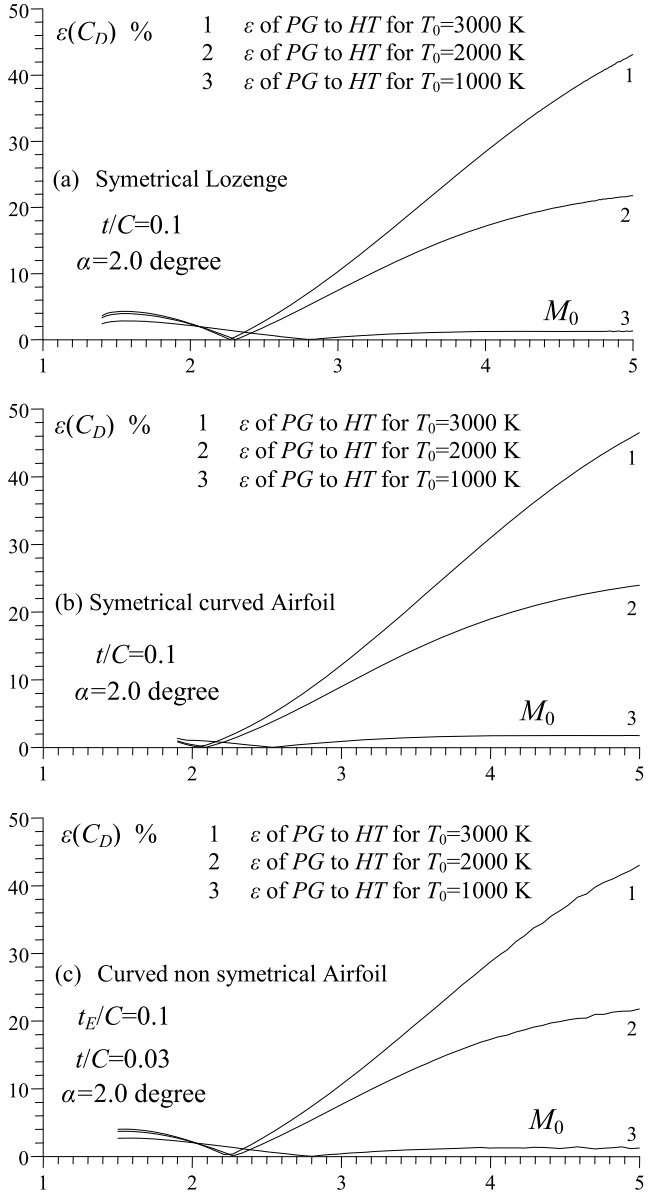

Fig. 25. Variation of the relative error caused by the PG model compared to HT model on the coefficient C_D versus M_0.

For M_0 given, there is a maximum deflection of the airfoil to avoid the detached shock. This limit also depends on T_0.

For each airfoil geometry, there is a minimum value of the upstream Mach number to avoid the detached shock. This limit depends on T_0, α and the gas used.

The T_0 is an essential parameter of our HT model. The PG model results do not depend on T_0.

The stagnation temperature T_0 degrades the C_D, C_L and C_m parameters compared to the PG models. This difference increases with the increase in T_0.

The maximum error is noticed on the coefficient C_L which can arrive at 39.38% when $T_0 = 3500$ K for the selected airfoils when $M_0 = 4.00$ and $\alpha = 2.00$ and can reach 59% when $T_0 = 3500$ K for $M_0 = 5.00$ and $\alpha = 2.00$.

For $t/C < 1.0$ or $M_0 < 2.00$ or $T_0 < 240$ K, the PG model can be used to evaluate the flow independently of the values of M_0 and T_0. But if $t/C > 1.0$ or $M_0 > 2.00$ or $T_0 > 240$ K, the corrections given by the HT model become necessary to evaluate the flow parameters accurately.

The PG model use limit in terms of maximum values of M_0, t/C, and T_0 is set to the required accuracy.

The presentation of the results on the choice of three airfoils differs. The developed program can do the calculation for any airfoil shape.

Not only do the parameters α, T_0, M_0, t/C influence the aerodynamic coefficients, the airfoil geometry also influences.

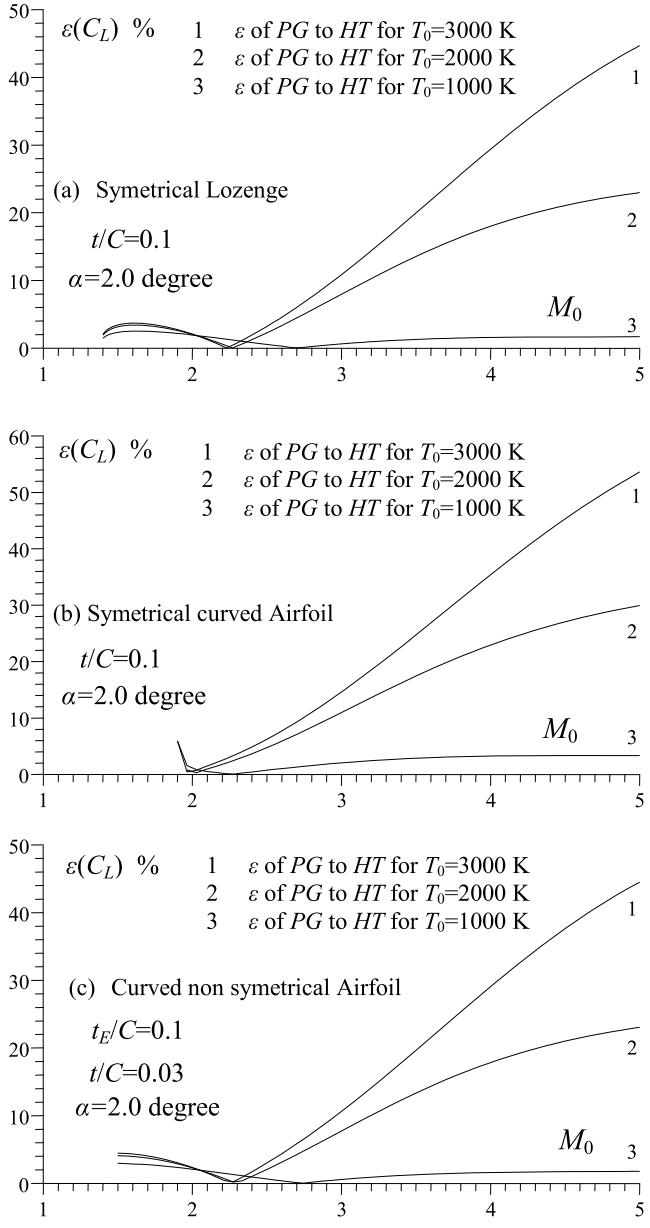

Fig. 26. Variation of the relative error caused by the PG model compared to HT model on the coefficient C_L versus M_0.

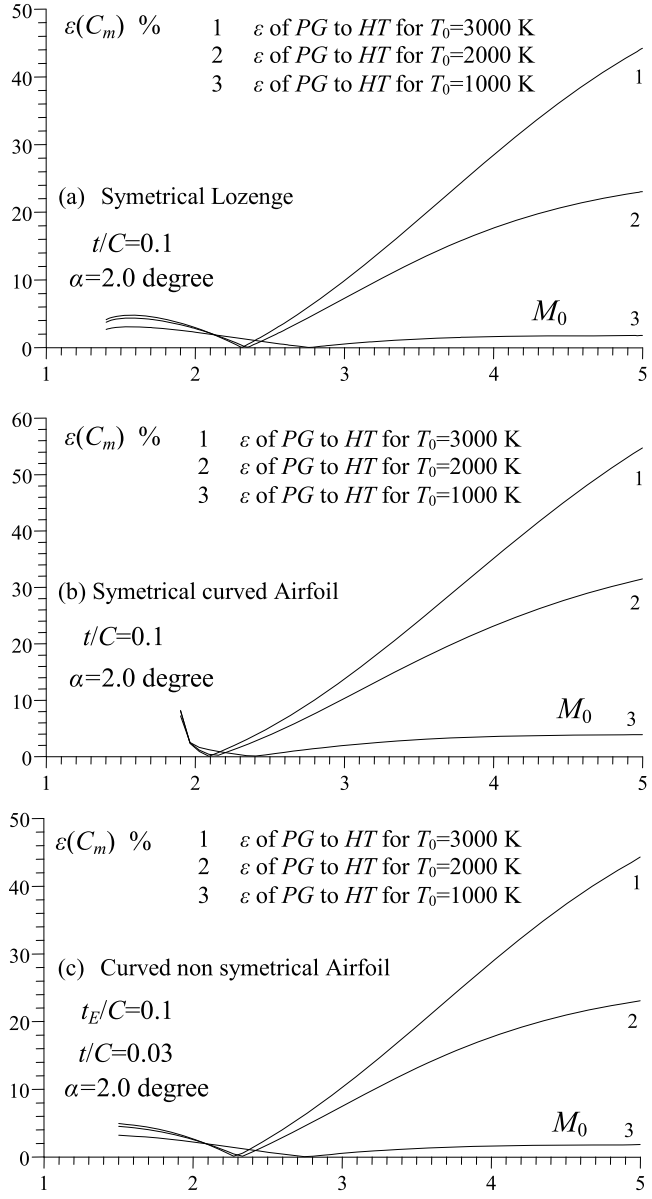

Fig. 27. Variation of the relative error caused by the PG model compared to HT model on the coefficient C_m versus M_0.

The flow around an airfoil is characterized by the generation of a shock wave at the leading edge in addition to the possibility of having a progressive shock through the surface of a certain airfoil, like the third airfoil.

The flow around an airfoil is characterized by an entropy jump due to developed shock on the airfoil.

It can be considered that the work carried out can be considered as a numercial wind tunnel. It allows to numerically validate the new HT model with the old existing PG model that is experimentally validated.

As a perspective, this problem can be studied for the airfoils having a slat and ailerons to have a more maneuverability for the variation of the aerodynamic coefficients.

Nomenclature

θ	Deviation angle of an airfoil segment
ψ	Flow angle deviation
M	Mach number
β	Shock wave deviation
μ	Mach angle
γ	Specific heats ratio
R	Thermodynamic constant of air
C_P	Specific heat at constant pressure
ν	Prandtl-Meyer function
α	Angle of incidence of the airfoil
D	Drag force
L	Lift force
m	Pitchnig moment

q_0	Dynamic pressure at upstream infinity
S	Reference surface
P	Pressure
T	Temperature
ρ	Density
C	Airfoil chord
C_m	Pitching moment coefficient
C_D	Drag coefficient
C_L	Lift coefficient
t	Maximum thickness of the airfoil
x, y	Position of the point on the airfoil.
ε	Error of computation
f_E	Equation of the airfoil extrados
f_I	Equation of the airfoil intrados
k	Nodes number on the extrados
l	Nodes number on the intrados
n	Total number of node on the airfoil
PG	Perfect gas
HT	High temperature
PM	Prandtl Meyer
ΔS	Total variation of entropy

Subscripts

0	Upstream condition
1	Upstream state at the panel under consideration
2	Considered panel
E	Extrados
I	Intrados
p	Point for the calculation of the pitching moment

Acknowledgments. The authors acknowledges Khaoula, Abdel-Ghani Amine, Ritadj and Assil Zebbiche and Mouza Ouahiba for granting time to prepare this manuscript.

References

[1] J. Moran, Introduction to theoretical and computational aerodynamics, John Wiley & Sons, New York, USA, 1984
[2] I.H. Abbott, A.E. VonDoenhoff, Theory of wing sections including summary of airfoil, Dover Publication, Inc., New York, 1959
[3] G. Emanuel, Gasdynamic: theory and application, AIAA Educational Series, New York, 1986
[4] J.D.Jr. Anderson, Fundamentals of aerodynamics, 2nd Edn, McGraw-Hill Book Company, New York, USA, 1988
[5] J.D.Jr. Anderson, Modern compressible flow with historical perspective, 2nd Edn, McGraw-Hill Book Company, New York, USA, 1982
[6] J.D.Jr. Anderson, Hypersonic and high temperature gas dynamics, McGraw-Hill Book Company, New York, 1989
[7] M.J. Zucro, J.D. Hoffman, Gas dynamics, Wiley, New York, Vol. 1 and 2 , 1976
[8] T. Zebbiche, Z. Youbi, Effect of stagnation temperature on the supersonic flow parameters with application for air in nozzles, Aeronaut. J. 111 (2007) 31–40
[9] T. Zebbiche, Z. Youbi, Supersonic flow parameters at high temperature. application for air in nozzles, German Aerospace Congress 2005, DGLR-2005-0256, Friendrichshafen, Germany, 2005
[10] E.T. Kenneth, Computation of thermally perfect properties of oblique shcok waves, NASA CR- 4749 1996
[11] E.T. Kenneth, Computation of thermally perfect oblique shcok waves properties, AIAA-97-0868, 35th Aerospace Sciences Meeting and Exhibit, Aerospace Sciences Meetings, 1997
[12] K.E. Tatum, Computation of thermally perfect oblique shock wave properties, 35th Aerospace Sciences Meeting and Exhibit, Reno, AIAA-97-0868 1997
[13] S.M. Yahya, Gas tables for compressible flow calculation, Fifth edition, New Age International Publishers, New Delhi, 2006
[14] T. Zebbiche, Effect of stagnation temperature on the normal shock wave, Int. J. Aeronaut. Space Sci. 10 (2009) 1–14
[15] C.R. Peterson, P.G. Hill, Mechanics and thermodynamics of propulsion, Addition-Wesley Publishing Company Inc., New York, USA, 1965
[16] G.P. Sutton, O. Biblarz, Rocket propulsion elements, 8ème Édn, John Wiley and Sons, New York, USA, 2010
[17] T. Zebbiche, M. Salhi, M. Boun-jad, Numerical computation of supersonic flow around a pointed airfoils, J. Comput. Methods Sci. Eng. 12 (2012) 213–233.
[18] G.J. Van Wylen, Fundamentals of classical thermodynamics, John Wiley and Sons, Inc., New York, USA, 1973
[19] B.J. McBride, S. Gordon, M.A. Reno, Thermodynamic Data for Fifty Reference Elements, NASA TP- 3287, 1993
[20] T. Zebbiche, Stagnation temperature effect on the Prandtl Meyer function, AIAA J. 45 (2007) 952–954
[21] T. Zebbiche, M. Boun-jad, Numerical quadrature for the Prandtl–Meyer function at high temperature with application for air, Thermophys. Aeromech. 19 (2012) 381–384
[22] A. Raltson, A. Rabinowitz, A First Course in Numerical Analysis, McGraw Hill Book Company, New York, USA, 1985
[23] A. Iserles, A first course in the numerical analysis of differential equations, Cambridge University Press, London, UK, 1996
[24] B. Démidovitch, I. Maron, Eléments de calcul numérique, Editions MIR, Moscow, Russia, 1987

Cite this article as: R. Takhnouni, T. Zebbiche, A. Allali, Stagnation temperature effect on the supersonic flow around pointed airfoils with application for air, Mechanics & Industry **19**, 312 (2018)